Negative Absolute Temperature for Motional Degrees of Freedom

S. Braun *et al.*

Science **339**, 52 (2013);
DOI: 10.1126/science.1227831

17. S. Kumar, J. E. Pringle, *Mon. Not. R. Astron. Soc.* **213**, 435 (1985).
18. R. P. Nelson, J. C. B. Papaloizou, *Mon. Not. R. Astron. Soc.* **315**, 570 (2000).
19. We typically set $GM = c = 1$, where c is the speed of light, G is the gravitational constant, and M is the mass of the BH, so that $r_g \equiv GM/c^2 = 1$. For dimensional clarity, these constants are sometimes reintroduced.
20. S. A. Balbus, J. F. Hawley, *Astrophys. J.* **376**, 214 (1991).
21. P. C. Fragile, O. M. Blaes, P. Anninos, J. D. Salmonson, *Astrophys. J.* **668**, 417 (2007).
22. M. C. Begelman, R. D. Blandford, M. J. Rees, *Nature* **287**, 307 (1980).
23. A. Perego, M. Dotti, M. Colpi, M. Volonteri, *Mon. Not. R. Astron. Soc.* **399**, 2249 (2009).
24. T. Bogdanović, C. S. Reynolds, M. C. Miller, *Astrophys. J.* **661**, L147 (2007).
25. P. Natarajan, P. J. Armitage, *Mon. Not. R. Astron. Soc.* **309**, 961 (1999).
26. N. Stone, A. Loeb, *Phys. Rev. Lett.* **108**, 061302 (2012).
27. A. R. King, J. P. Lasota, *Astron. Astrophys.* **58**, 175 (1977).
28. J. C. McKinney, A. Tchekhovskoy, R. D. Blandford, *Mon. Not. R. Astron. Soc.* **423**, 3083 (2012).
29. H. Kim, H. K. Lee, C. H. Lee, *J. Cosmol. Astropart. Phys.* **2003**, 1 (2003).
30. A. R. King, in *Magnetic Fields in the Universe: From Laboratory and Stars to Primordial Structures*, E. M. de Gouveia dal Pino, G. Lugones, A. Lazarian, Eds. (American Institute of Physics, Melville, NY, 2005), pp. 175–182.
31. C. Palenzuela, T. Garrett, L. Lehner, S. L. Liebling, *Phys. Rev. D* **82**, 044045 (2010).
32. V. Semenov, S. Dyadechkin, B. Punsly, *Science* **305**, 978 (2004).
33. See supplementary materials on *Science* Online.
34. A. Tchekhovskoy, J. C. McKinney, *Mon. Not. R. Astron. Soc.* **423**, L55 (2012).
35. Spins of $j \sim 0.9$ give mid-range BH rotation rates. See the Physical Models section in the supplement.
36. The magnetic field built up via direct magnetic flux advection, but the buildup might also occur via dynamo generation, as seen in our prior untilted simulations that showed emergent large-scale dipolar flux patches.
37. R. Narayan, I. Yi, R. Mahadevan, *Nature* **374**, 623 (1995).
38. J. S. Bloom *et al.*, *Science* **333**, 203 (2011).
39. R. C. Reis *et al.*, *Science* **337**, 949 (2012).

Acknowledgments: J.C.M. thanks R. Narayan, J. Dexter, and P. C. Fragile for useful discussions, and R. Kaehler at KIPAC (SLAC/Stanford) for the artistic rendering in fig. S1. Supported by NASA Fermi grant NNX11AO21G (J.C.M.), a Princeton Center for Theoretical Science fellowship (A.T.), and NSF Extreme Science and Engineering Discovery Environment resources provided by the Texas Advanced Computing Center (Lonestar/Ranch) and the National Institute for Computational Sciences (Kraken) under awards TG-PHY120005 (J.C.M.) and TG-AST100040 (A.T.) and provided by NASA Advanced Supercomputing (Pleiades) for the Fermi grant. GRMHD simulation data are contained in Table 1 and tables S1 and S2. A.T. is a Princeton Center for Theoretical Science Fellow.

Supplementary Materials

www.sciencemag.org/cgi/content/full/science.1230811/DC1
Materials and Methods
Fig. S1
Tables S1 and S2
Movies S1 and S2
References (*40*–*98*)

27 September 2012; accepted 7 November 2012
Published online 15 November 2012;
10.1126/science.1230811

Negative Absolute Temperature for Motional Degrees of Freedom

S. Braun,[1,2] J. P. Ronzheimer,[1,2] M. Schreiber,[1,2] S. S. Hodgman,[1,2] T. Rom,[1,2] I. Bloch,[1,2] U. Schneider[1,2]*

Absolute temperature is usually bound to be positive. Under special conditions, however, negative temperatures—in which high-energy states are more occupied than low-energy states—are also possible. Such states have been demonstrated in localized systems with finite, discrete spectra. Here, we prepared a negative temperature state for motional degrees of freedom. By tailoring the Bose-Hubbard Hamiltonian, we created an attractively interacting ensemble of ultracold bosons at negative temperature that is stable against collapse for arbitrary atom numbers. The quasimomentum distribution develops sharp peaks at the upper band edge, revealing thermal equilibrium and bosonic coherence over several lattice sites. Negative temperatures imply negative pressures and open up new parameter regimes for cold atoms, enabling fundamentally new many-body states.

Absolute temperature T is one of the central concepts of statistical mechanics and is a measure of, for example, the amount of disordered motion in a classical ideal gas. Therefore, nothing can be colder than $T = 0$, where classical particles would be at rest. In a thermal state of such an ideal gas, the probability P_i for a particle to occupy a state i with kinetic energy E_i is proportional to the Boltzmann factor

$$P_i \propto e^{-E_i/k_B T} \quad (1)$$

where k_B is Boltzmann's constant. An ensemble at positive temperature is described by an occupation distribution that decreases exponentially with energy. If we were to extend this formula to negative absolute temperatures, exponentially increasing distributions would result. Because the distribution needs to be normalizable, at positive temperatures a lower bound in energy is required, as the probabilities P_i would diverge for $E_i \to -\infty$. Negative temperatures, on the other hand, demand an upper bound in energy (*1*, *2*). In daily life, negative temperatures are absent, because kinetic energy in most systems, including particles in free space, only provides a lower energy bound. Even in lattice systems, where kinetic energy is split into distinct bands, implementing an upper energy bound for motional degrees of freedom is challenging, because potential and interaction energy need to be limited as well (*3*, *4*). So far, negative temperatures have been realized in localized spin systems (*5*–*7*), where the finite, discrete spectrum naturally provides both lower and upper energy bounds. Here, we were able to realize a negative temperature state for motional degrees of freedom.

In Fig. 1A, we schematically show the relation between entropy S and energy E for a thermal system possessing both lower and upper energy bounds. Starting at minimum energy, where only the ground state is populated, an increase in energy leads to an occupation of a larger number of states and therefore an increase in entropy. As the temperature approaches infinity, all states become equally populated and the entropy reaches its maximum possible value S_{max}. However, the energy can be increased even further if high-energy states are more populated than low-energy ones. In this regime, the entropy decreases with energy, which, according to the thermodynamic definition of temperature (*8*) ($1/T = \partial S/\partial E$), results in negative temperatures. The temperature is discontinuous at maximum entropy, jumping from positive to negative infinity. This is a consequence of the historic definition of temperature. A continuous and monotonically increasing temperature scale would be given by $-\beta = -1/k_B T$, also emphasizing that negative temperature states are hotter than positive temperature states, i.e., in thermal contact, heat would flow from a negative to a positive temperature system.

Because negative temperature systems can absorb entropy while releasing energy, they give rise to several counterintuitive effects, such as Carnot engines with an efficiency greater than unity (*4*). Through a stability analysis for thermodynamic equilibrium, we showed that negative temperature states of motional degrees of freedom necessarily possess negative pressure (*9*) and are thus of fundamental interest to the description of dark energy in cosmology, where negative pressure is required to account for the accelerating expansion of the universe (*10*).

Cold atoms in optical lattices are an ideal system to create negative temperature states because of the isolation from the environment and independent control of all relevant parameters (*11*). Bosonic atoms in the lowest band of a

[1]Fakultät für Physik, Ludwig-Maximilians-Universität München, Schellingstraße 4, 80799 Munich, Germany. [2]Max-Planck-Institut für Quantenoptik, Hans-Kopfermann-Straße 1, 85748 Garching, Germany.

*To whom correspondence should be addressed. E-mail: ulrich.schneider@lmu.de.

sufficiently deep optical lattice are described by the Bose-Hubbard Hamiltonian (*12*)

$$H = -J\sum_{\langle i,j\rangle}\hat{b}_i^\dagger\hat{b}_j + \frac{U}{2}\sum_i \hat{n}_i(\hat{n}_i - 1) + V\sum_i \mathrm{r}_i^2\hat{n}_i \quad (2)$$

Here, J is the tunneling matrix element between neighboring lattice sites $\langle i,j\rangle$, and $\hat{b}_i$ and $\hat{b}_i^\dagger$ are the annihilation and creation operator, respectively, for a boson on site i, U is the on-site interaction energy, $\hat{n}_i = \hat{b}_i^\dagger\hat{b}_i$ is the local number operator, and $V \propto \omega^2$ describes the external harmonic confinement, with r_i denoting the position of site i with respect to the trap center and ω the trap frequency.

In Fig. 1B, we show how lower and upper bounds can be realized for the three terms in the Hubbard Hamiltonian. The restriction to a single band naturally provides lower and upper bounds for the kinetic energy E_{kin}, but the interaction term E_{int} presents a challenge: Because in principle all bosons could occupy the same lattice site, the interaction energy can diverge in the thermodynamic limit. For repulsive interactions ($U > 0$), the interaction energy is only bounded from below but not from above, thereby limiting the system to positive temperatures; in contrast, for attractive interactions ($U < 0$), only an upper bound for the interaction energy is established, rendering positive temperature ensembles unstable. The situation is different for the Fermi-Hubbard model, where the Pauli principle enforces an upper limit on the interaction energy per atom of $U/2$ and thereby allows negative temperatures even in the repulsive case (*13*, *14*). Similarly, a trapping potential $V > 0$ only provides a lower bound for the potential energy E_{pot}, whereas an

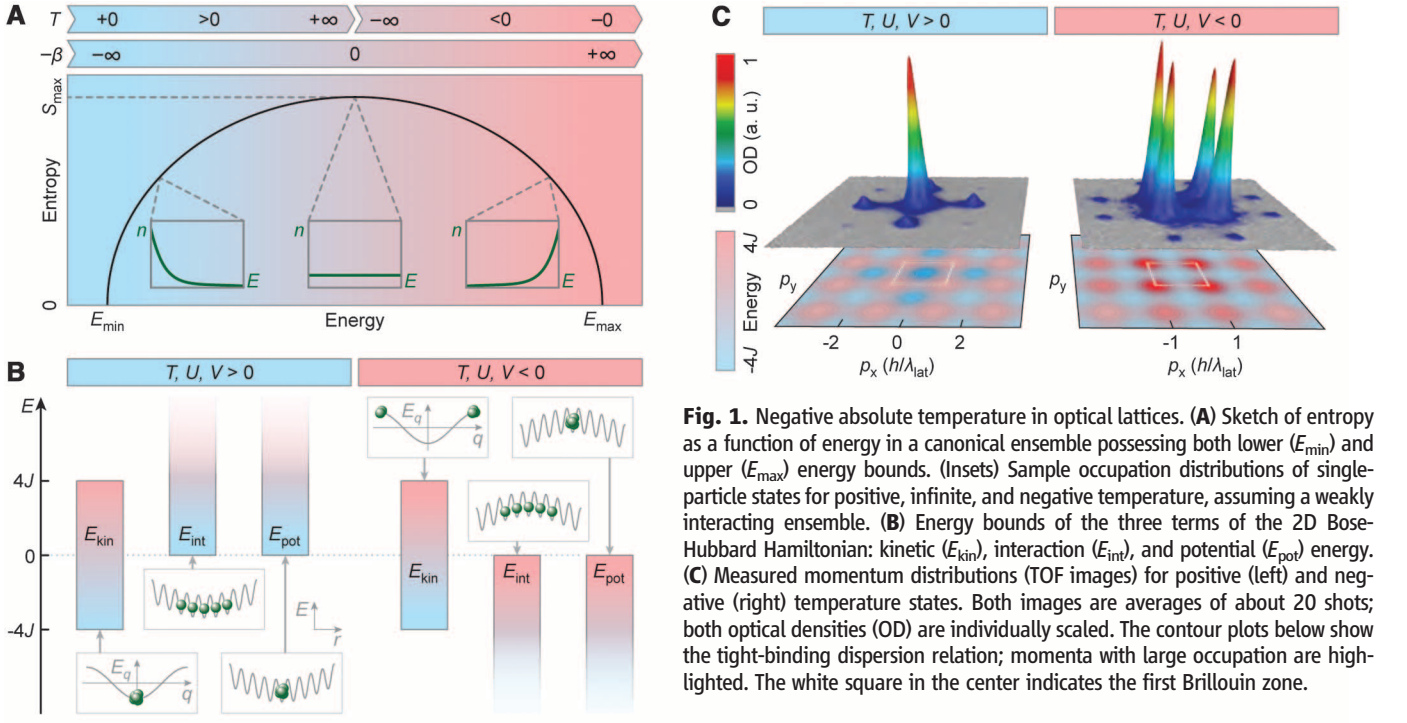

Fig. 1. Negative absolute temperature in optical lattices. (**A**) Sketch of entropy as a function of energy in a canonical ensemble possessing both lower (E_{min}) and upper (E_{max}) energy bounds. (Insets) Sample occupation distributions of single-particle states for positive, infinite, and negative temperature, assuming a weakly interacting ensemble. (**B**) Energy bounds of the three terms of the 2D Bose-Hubbard Hamiltonian: kinetic (E_{kin}), interaction (E_{int}), and potential (E_{pot}) energy. (**C**) Measured momentum distributions (TOF images) for positive (left) and negative (right) temperature states. Both images are averages of about 20 shots; both optical densities (OD) are individually scaled. The contour plots below show the tight-binding dispersion relation; momenta with large occupation are highlighted. The white square in the center indicates the first Brillouin zone.

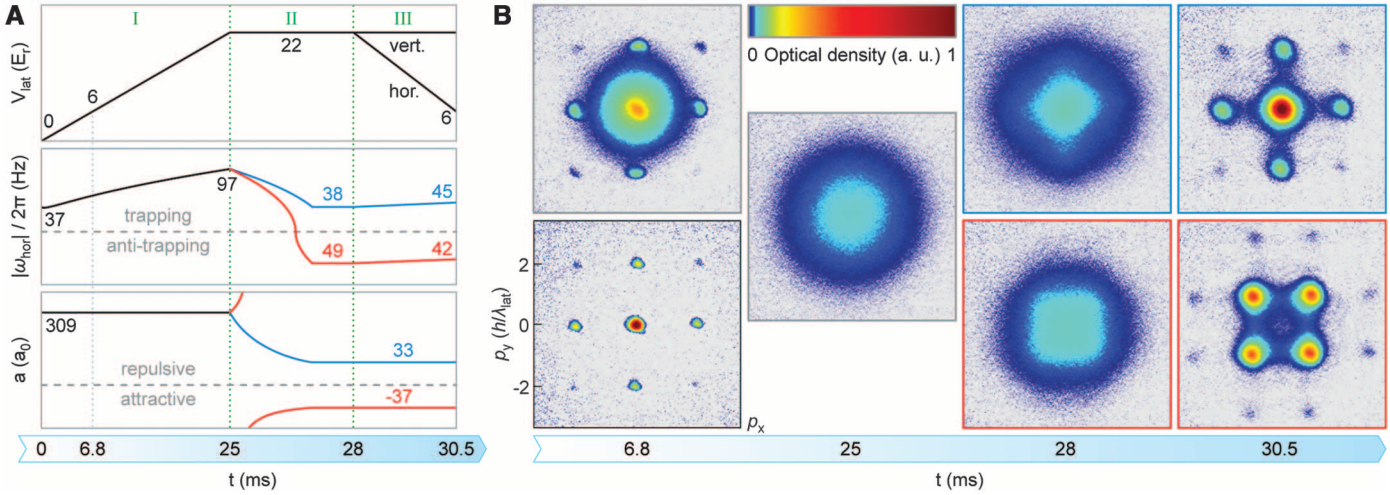

Fig. 2. Experimental sequence and TOF images. (**A**) Top to bottom: lattice depth, horizontal trap frequency, and scattering length as a function of time. Blue indicates the sequence for positive, red for negative temperature of the final state. (**B**) TOF images of the atomic cloud at various times t in the sequence. Blue borders indicate positive, red negative temperatures. The initial picture in a shallow lattice at $t = 6.8$ ms is taken once for a scattering length of $a = 309(5)\ a_0$ (top) as in the sequence, and once for $a = 33(1)\ a_0$ (bottom; OD rescaled by a factor of 0.25), comparable to the final images. All images are averages of about 20 individual shots. See also Fig. 1C.

anti-trapping potential $V < 0$ creates an upper bound. Therefore, stable negative temperature states with bosons can exist only for attractive interactions and an anti-trapping potential.

To bridge the transition between positive and negative temperatures, we used the $n = 1$ Mott insulator (*15*) close to the atomic limit ($|U|/J \to \infty$), which can be approximated by a product of Fock states $|\Psi\rangle = \prod_i \hat{b}_i^\dagger |0\rangle$. Because this state is a many-body eigenstate in both the repulsive and the attractive case, it allows us to switch between these regimes, ideally without producing entropy. The employed sequence (Fig. 2A) is based on a proposal by Rapp *et al*. (*4*), building on previous ideas by Mosk (*3*). It essentially consists of loading a repulsively interacting Bose-Einstein condensate (BEC) into the deep Mott insulating regime (I in Fig. 2A), switching U and V to negative values (II), and finally melting the Mott insulator again by reducing $|U|/J$ (III). For comparison, we also created a final positive temperature state with an analog sequence.

The experiment started with a BEC of $1.1(2) \times 10^5$ ^{39}K atoms in a pure dipole trap with horizontal trap frequency ω_{dip} ($V > 0$) at positive temperature ($T > 0$) and a scattering length of $a = 309(5)\ a_0$, with a_0 the Bohr radius. We ramped up a three-dimensional (3D) optical lattice (I) with simple cubic symmetry to a depth of $V_{lat} = 22(1)\ E_r$. Here, $E_r = h^2/(2m\lambda_{lat}^2)$ is the recoil energy with Planck's constant h, the atomic mass m, and the lattice wavelength $\lambda_{lat} = 736.65$ nm. The blue-detuned optical lattice provides an overall anti-trapping potential with a formally imaginary horizontal trap frequency ω_{lat} that reduces the confinement of the dipole trap, giving an effective horizontal trap frequency $\omega_{hor} = (\omega_{dip}^2 + \omega_{lat}^2)^{1/2}$. Once the atoms are in the deep Mott insulating regime where tunneling can essentially be neglected [tunneling time $\tau = h/(2\pi J) = 10(2)$ ms], we set the desired attractive (repulsive) interactions (II) to prepare a final negative (positive) temperature state using a Feshbach resonance (*16*). Simultaneously, we decreased the horizontal confinement to an overall anti-trapping (trapping) potential by reducing ω_{dip}. Subsequently, we lowered the horizontal lattice depths (III), yielding a final value of $U/J = -2.1(1)$ [$U/J = +1.9(1)$], and probed the resulting momentum distribution by absorption imaging after 7 ms time-of-flight (TOF). The whole sequence was experimentally optimized to maximize the visibility of the final negative temperature state. We chose a 2D geometry for the final state to enable strong anti-trapping potentials and to avoid detrimental effects due to gravity (*9*).

In Fig. 2B, we show TOF images of the cloud for various times t in the sequence, indicated in Fig. 2A. During the initial lattice ramp [at $V_{lat} = 6.1(1)E_r$], interference peaks of the superfluid in the lattice can be observed ($t = 6.8$ ms) (Fig. 2B, top). Because quantum depletion caused by the strong repulsive interactions already reduces the visibility of the interference peaks in this image (*17*), we also show the initial superfluid for identical lattice and dipole ramps, but at a scattering length of $a = 33(1)\ a_0$ ($t = 6.8$ ms) (Fig. 2B, bottom). The interference peaks are lost as the Mott insulating regime is entered ($t = 25$ ms). In the deep lattice, only weak nearest-neighbor correlations are expected, resulting in similar images for both repulsive and attractive interactions ($t = 28$ ms). After reducing the horizontal lattice depths back into the superfluid regime, the coherence of the atomic sample emerges again. For positive temperatures, the final image at $t = 30.5$ ms is comparable, albeit somewhat heated, to the initial one at $t = 6.8$ ms, whereas for attractive interactions, sharp peaks show up in the corners of the first Brillouin zone, indicating macroscopic occupation of maximum kinetic energy. The spontaneous development of these sharp interference peaks is a striking signature of a stable negative temperature state for motional degrees of freedom. In principle, the system can enter the negative temperature regime following one of two routes: It either stays close to thermal equilibrium during the entire sequence or, alternatively, relaxes toward a thermal distribution during lattice ramp-down. Either way demonstrates the thermodynamic stability of this negative temperature state.

To examine the degree of thermalization in the final states, we used band-mapped (*18*) images and extracted the kinetic energy distribution, assuming a noninteracting lattice dispersion relation $E_{kin}(q_x,q_y)$. The result is shown in Fig. 3, displaying very good agreement with a fitted Bose-Einstein distribution. The fitted temperatures of $T = -2.2J/k_B$ and $T = 2.7J/k_B$ for the two cases only represent upper bounds for the absolute values $|T|$ of the average temperature because the fits neglect the inhomogeneous filling of the sample (*9*). Both temperatures are slightly larger than the critical temperature $|T_{BKT}| \approx 1.8J/k_B$ (*19*) for the superfluid transition in an infinite 2D system but lie below the condensation temperature $|T_C| = 3.4(2)J/k_B$ of noninteracting

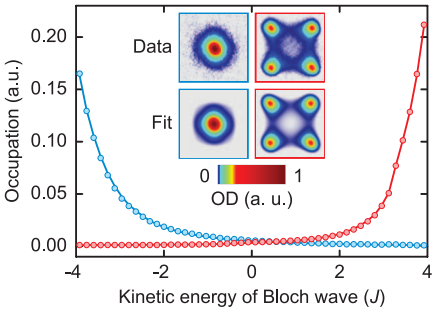

Fig. 3. Occupation distributions. The occupation of the kinetic energies within the first Brillouin zone is plotted for the final positive (blue) and negative (red) temperature states. Points show experimental data extracted from band-mapped pictures. Solid lines are fits to a noninteracting Bose-Einstein distribution assuming a homogeneous system. **(Insets)** Top row: Symmetrized positive (left) and negative (right) temperature images of the quasimomentum distribution in the horizontal plane. Bottom row: Fitted distributions for the two cases. All distributions are broadened by the in situ cloud size (*9*).

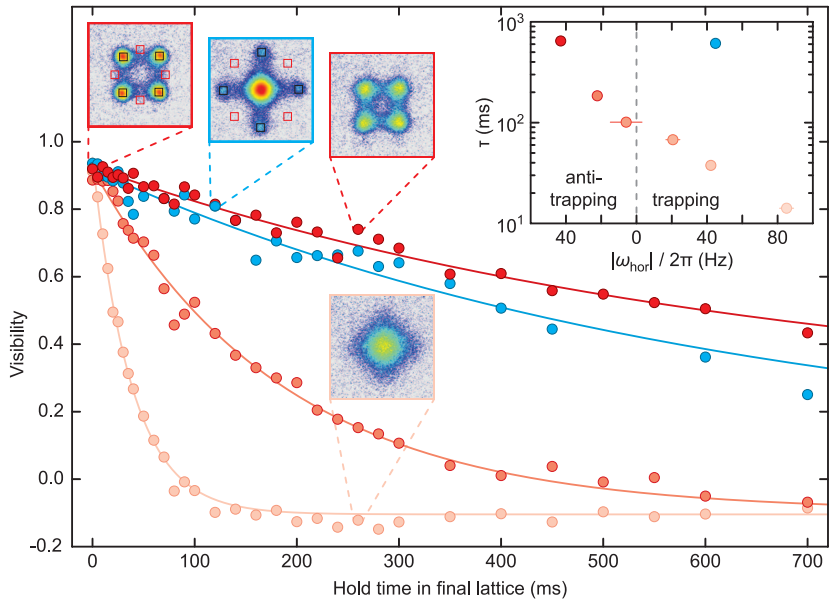

Fig. 4. Stability of the positive (blue) and negative (red) temperature states. Main figure: Visibility $V = (n_b - n_r)/(n_b + n_r)$ extracted from the atom numbers in the black (n_b) and red (n_r) boxes (indicated in the TOF images) plotted versus hold time in the final state for various horizontal trap frequencies. Dark red, $|\omega_{hor}|/2\pi = 43(1)$ Hz anti-trapping; medium red, 22(3) Hz anti-trapping; light red, 42(3) Hz trapping; blue, 45(3) Hz trapping. **(Inset)** Coherence lifetimes τ extracted from exponential fits (solid lines in main figure). The statistical error bars from the fits are smaller than the data points. The color scale of the images is identical to Fig. 2B (see also fig. S3).

bosons in a 2D harmonic trap for the given average density (*9*).

Ideally, entropy is produced during the sequence only in the superfluid/normal shell around the interim Mott insulator: While ramping to the deep lattice, the atoms in this shell localize to individual lattice sites and can subsequently be described as a $|T| = \infty$ system (*14*). Numerical calculations have shown that the total entropy produced in this process can be small (*4*), because most of the atoms are located in the Mott insulating core. We attribute the observed additional heating during the sequence to nonadiabaticities during lattice ramp-down and residual double occupancies in the interim Mott insulator.

In principle, the coherence length of the atomic sample can be extracted from the interference pattern recorded after a long TOF (*20*). However, the experiment was limited to finite TOF, where the momentum distribution is convolved with the initial spatial distribution. By comparing the measured TOF images with theoretically expected distributions, we were able to extract a coherence length in the final negative temperature state of three to five lattice constants (*9*).

To demonstrate the stability of the observed negative temperature state, Fig. 4 shows the visibility of the interference pattern as a function of hold time in the final lattice. The resulting lifetime of the coherence in the final negative temperature state crucially depends on the horizontal trap frequencies (inset): Lifetimes exceed τ = 600 ms for an optimally chosen anti-trapping potential, but an increasingly fast loss of coherence is visible for less anti-trapping geometries. In the case of trapping potentials, the ensemble can even return to metastable positive temperatures, giving rise to the small negative visibilities observed after longer hold times (fig. S4). The loss of coherence probably originates from a mismatch between the attractive mean field and the external potential, which acts as an effective potential and leads to fast dephasing between lattice sites.

The high stability of the negative temperature state for the optimally chosen anti-trapping potential indicates that the final chemical potential is matched throughout the sample such that no global redistribution of atoms is necessary. The remaining slow decay of coherence is not specific to the negative temperature state because we also observe comparable heating for the corresponding positive temperature case (blue data in Fig. 4), as well as the initial superfluid in the lattice. It probably originates from three-body losses and light-assisted collisions. In contrast to metastable excited states (*21*), this isolated negative temperature ensemble is intrinsically stable and cannot decay into states at lower kinetic energies. It represents a stable bosonic ensemble at attractive interactions for arbitrary atom numbers; the negative temperature stabilizes the system against mean-field collapse that is driven by the negative pressure.

Negative temperature states can be exploited to investigate the Mott insulator transition (*22*) as well as the renormalization of Hubbard parameters (*23, 24*) for attractive interactions. As the stability of the attractive gas relies on the bounded kinetic energy in the Hubbard model, it naturally allows a controlled study of the transition from stable to unstable by lowering the lattice depth, thereby connecting this regime with the study of collapsing BECs (*25*), which is also of interest for cosmology (*26*). Negative temperatures also considerably enhance the parameter space accessible for quantum simulations in optical lattices, because they enable the study of new many-body systems whenever the bands are not symmetric with respect to the inversion of kinetic energy. This is the case, for example, in triangular or Kagomé lattices, where in current implementations (*27*) the interesting flat band is the highest of three sub-bands. In fermionic systems, negative temperatures enable, for example, the study of the attractive three-component model with symmetric interactions [SU(3)] describing color superfluidity and trion (baryon) formation using repulsive ^{173}Yb (*28*), where low losses and symmetric interactions are expected but magnetic Feshbach resonances are absent.

References and Notes

1. N. F. Ramsey, *Phys. Rev.* **103**, 20 (1956).
2. M. J. Klein, *Phys. Rev.* **104**, 589 (1956).
3. A. P. Mosk, *Phys. Rev. Lett.* **95**, 040403 (2005).
4. A. Rapp, S. Mandt, A. Rosch, *Phys. Rev. Lett.* **105**, 220405 (2010).
5. E. M. Purcell, R. V. Pound, *Phys. Rev.* **81**, 279 (1951).
6. A. S. Oja, O. V. Lounasmaa, *Rev. Mod. Phys.* **69**, 1 (1997).
7. P. Medley, D. M. Weld, H. Miyake, D. E. Pritchard, W. Ketterle, *Phys. Rev. Lett.* **106**, 195301 (2011).
8. K. Huang, *Statistical Mechanics* (Wiley, New York, ed. 2, 1987).
9. See supplementary materials on *Science* Online.
10. J. A. Frieman, M. S. Turner, D. Huterer, *Annu. Rev. Astron. Astrophys.* **46**, 385 (2008).
11. I. Bloch, J. Dalibard, W. Zwerger, *Rev. Mod. Phys.* **80**, 885 (2008).
12. D. Jaksch, C. Bruder, J. I. Cirac, C. W. Gardiner, P. Zoller, *Phys. Rev. Lett.* **81**, 3108 (1998).
13. N. Tsuji, T. Oka, P. Werner, H. Aoki, *Phys. Rev. Lett.* **106**, 236401 (2011).
14. U. Schneider *et al.*, *Nat. Phys.* **8**, 213 (2012).
15. M. Greiner, O. Mandel, T. Esslinger, T. W. Hänsch, I. Bloch, *Nature* **415**, 39 (2002).
16. M. Zaccanti *et al.*, *Nat. Phys.* **5**, 586 (2009).
17. K. Xu *et al.*, *Phys. Rev. Lett.* **96**, 180405 (2006).
18. A. Kastberg, W. D. Phillips, S. L. Rolston, R. J. C. Spreeuw, P. S. Jessen, *Phys. Rev. Lett.* **74**, 1542 (1995).
19. B. Capogrosso-Sansone, S. G. Söyler, N. Prokof'ev, B. Svistunov, *Phys. Rev. A* **77**, 015602 (2008).
20. F. Gerbier *et al.*, *Phys. Rev. Lett.* **101**, 155303 (2008).
21. E. Haller *et al.*, *Science* **325**, 1224 (2009).
22. M. J. Mark *et al.*, *Phys. Rev. Lett.* **108**, 215302 (2012).
23. S. Will *et al.*, *Nature* **465**, 197 (2010).
24. J. Heinze *et al.*, *Phys. Rev. Lett.* **107**, 135303 (2011).
25. E. A. Donley *et al.*, *Nature* **412**, 295 (2001).
26. T. Fukuyama, M. Morikawa, T. Tatekawa, *J. Cosmol. Astropart. Phys.* **2008**, 033 (2008).
27. G.-B. Jo *et al.*, *Phys. Rev. Lett.* **108**, 045305 (2012).
28. Á. Rapp, *Phys. Rev. A* **85**, 043612 (2012).

Acknowledgments: We thank A. Rapp, A. Rosch, S. Mandt, and W. Hofstetter for helpful discussions and D. Garbe for technical assistance. We acknowledge financial support by the Deutsche Forschungsgemeinschaft (FOR801, Deutsch-Israelisches Kooperationsprojekt Quantum phases of ultracold atoms in optical lattices), the U.S. Defense Advanced Research Projects Agency Optical Lattice Emulator program, and Nanosystems Initiative Munich.

Supplementary Materials

www.sciencemag.org/cgi/content/full/339/6115/52/DC1
Supplementary Text
Figs. S1 to S4
References (*29–38*)

23 July 2012; accepted 6 November 2012
10.1126/science.1227831

Current-Driven Spin Dynamics of Artificially Constructed Quantum Magnets

Alexander Ako Khajetoorians,[1]* Benjamin Baxevanis,[2] Christoph Hübner,[2] Tobias Schlenk,[1] Stefan Krause,[1] Tim Oliver Wehling,[3,4] Samir Lounis,[5] Alexander Lichtenstein,[2] Daniela Pfannkuche,[2] Jens Wiebe,[1]* Roland Wiesendanger[1]

The future of nanoscale spin-based technologies hinges on a fundamental understanding and dynamic control of atomic-scale magnets. The role of the substrate conduction electrons on the dynamics of supported atomic magnets is still a question of interest lacking experimental insight. We characterized the temperature-dependent dynamical response of artificially constructed magnets, composed of a few exchange-coupled atomic spins adsorbed on a metallic substrate, to spin-polarized currents driven and read out by a magnetic scanning tunneling microscope tip. The dynamics, reflected by two-state spin noise, is quantified by a model that considers the interplay between quantum tunneling and sequential spin transitions driven by electron spin-flip processes and accounts for an observed spin-transfer torque effect.

For magnetic storage technology (*1*), where magnets represent bits of information (*2*, *3*), effective manipulation of the magnetization without a magnetic field is of crucial importance. All-electrical manipulation offers technological advantages, such as highly localized bit control